Cellulose (2022) 29:5659–5676
https://doi.org/10.1007/s10570-022-04624-4

ORIGINAL RESEARCH

Multifunctional natural fibers: the potential of core shell MgO–SiO_2 nanoparticles

Joana C. Araújo · Pilar Teixeira · Raul Fangueiro · Diana P. Ferreira

Received: 25 February 2022 / Accepted: 26 April 2022 / Published online: 17 May 2022

Abstract Core–shell nanoparticles (NPs) based on metal oxides, namely magnesium oxide (MgO) and silica (SiO_2), are a fantastic alternative for natural fibers' functionalization. In this work, flax fibers were functionalized with MgO and MgO–SiO_2 core–shell NPs to achieve multifunctionality. The flax fabrics were functionalized with both NPs by a simple in-situ method. Parallelly, the synthesis of the isolated NPs was performed for comparison purposes. The developed samples were characterized, confirming the successful synthesis of the core–shell NPs and their incorporation onto the fabrics. The wash durability tests confirmed the beneficial effect of the SiO_2 shell on the NPs' anchorage. Ultraviolet (UV) protection capability (UV protection factor (UPF) of 50+) and hydrophobicity (water contact angle (WCA) of 123.0°) were achieved, together with antibacterial activity and the degradation of methylene blue (MB) capability. Overall, this work presents an innovative method for the synthesis of MgO–SiO_2 core–shell NPs and their incorporation onto flax fabrics.

Keywords In-situ synthesis · Core–shell nanoparticles · Natural fibers · Antibacterial activity · Hydrophobicity · Photodegradation

J. C. Araújo · R. Fangueiro · D. P. Ferreira (✉)
Centre for Textile Science and Technology (2C2T), University of Minho, 4800 Guimarães, Portugal
e-mail: diana.ferreira@det.uminho.pt

P. Teixeira
CEB - Centre of Biological Engineering, University of Minho, 4710-057 Braga, Portugal

P. Teixeira
LABBELS –Associate Laboratory, Guimarães, Portugal

R. Fangueiro
Department of Textile Engineering, University of Minho, Guimarães, Portugal

Introduction

Metal oxide NPs, such as zinc oxide (ZnO), titanium oxide (TiO_2), calcium oxide (CaO), copper oxide (CuO), tin oxide (SnO_2) and specially MgO NPs show unique chemical and physical properties, making them great candidates to be used in several fields like, materials chemistry, medicine, agriculture, electronics, catalysis, among others (Chavali and Nikolova 2019). MgO NPs are one of the most important functional materials. This metal oxide occurs in nature as a colourless and crystalline mineral and can easily be produced in large-scale. MgO NPs present outstanding characteristics, namely a great refractive index, resistance to corrosion, high thermal conductivity, stability and high optical transparency. Besides these excellent properties, MgO NPs are also well-known because of their antibacterial, antioxidant and anticancer activity (Abinaya et al. 2021).

These particles are also biocompatible and non-toxic, being one of the safest inorganic materials,

which is of great importance for textile applications since they are in direct contact with the user (Karthikeyan et al. 2021). The multifunctionality of MgO NPs in combination with their low cost, makes them great candidates to be used in several areas, as adsorbents for wastewater and heavy metal treatment, hydrogen storage, chemical and biological sensors, solar cells, electroluminescence sensors, etc. (Wahab et al. 2018).

Concurrently, SiO_2 NPs also present exceptional characteristics, large surface area, easy synthesis, rich surface chemistry, biocompatibility and tunable properties, like optoelectronic, mechanical and chemical stability (Prabha et al. 2021). Additionally, SiO_2 NPs can be combined with a wide array of materials (Jeelani et al. 2019). SiO_2 when added to other metal oxides can enhance their properties, due to its high active surface (Gunathilake and Jaroniec 2014).

Simple NPs are well known materials because of their excellent properties. However, other type of NPs constituted by two or more materials, composite and core–shell, are attracting more and more attention. Core–shell nanoparticles can be defined as materials that are composed by a core (inner material) and a shell (outer layer material). These particles are highly functional, with altered properties. The resulting functionalities of core–shell nanoparticles can be modified changing the core or the shell materials and even its ratio. For example, the reactivity of the core material can decrease as a result of the shell material coating, which causes an increase of the core's stability and dispersibility (Chaudhuri and Paria 2012).

Being that SiO_2 NPs present a high surface reactivity, because of the presence of a high number of silanol groups, which can change the surface charge of the other metal oxide and improve the adhesion of the NPs onto the substrate, they are great materials to be used as shell materials for the functionalization of natural fibers (Hoang et al. 2018). Therefore, the production of MgO–SiO_2 core–shell nanoparticles can be a great strategy to not only combine their functionalities, but also to improve the anchorage of the NPs onto fibrous structures.

The incorporation of NPs, namely metal oxides, is a great alternative for the functionalization of textiles, due their nanoscale, good structural characteristics and high oxidation potential (Araújo et al. 2021). This functionalization can provide several properties, such as UV protection, easy/self-cleaning, antibacterial activity and the adsorption/decomposition of harmful agents (Araújo et al. 2020). For this specific application, MgO NPs have been gaining special attention due to their high surface area, large number of reactive sites, high absorption capacity and decomposition ability (Vu et al. 2016). However, the functionalization of textile substrates with nanomaterials still presents a major drawback: the poor adhesion or even chemical bonding of the NPs onto the fabrics' surface (Rivero et al. 2015). Several methods can be used in order to overcome this problem, such as the use of binding agents or polymers and fibers' treatments, but the in-situ synthesis of the particles, as well as the use of SiO_2 have arisen as better alternatives (Rivero et al. 2015; Araújo et al. 2020).

Natural fibers are a great example of a sustainable and adaptable substrate, since they are highly abundant, biodegradable, biocompatible and present good mechanical properties (Ferreira et al. 2018). Therefore, the functionalization of natural fibers with metal oxide core–shell NPs emerges as a great alternative for the development of multifunctional fibrous systems. One of the most promising natural fiber is flax, since it presents excellent mechanical properties, being widely used as reinforcements in composite materials (Costa et al. 2018). The use of non-toxic solvents and mild conditions is also very important in order to improve the sustainability of the processes.

Functionalities like UV protection, hydrophobicity, antibacterial activity and the degradation of harmful agents, such as dyes are of huge importance for protection applications. Sun exposure for prolonged periods of time and without protection, and being that the skin is the largest organ of the body, is the cause of several harmful effects like, sunburn, erythema, premature aging and even skin cancer (Koozekonan et al. 2021). Hydrophobic surfaces allow not only water resistance but also self-cleaning ability, avoiding the penetration of other aqueous solutions that may be harmful, being great materials for a wide range of applications (Chirila and Danila 2021). Diseases caused by bacteria are one of the biggest issues related to public health, being the cause of several deaths (Yu et al. 2021). Another problem for human health is dyes originated from the dye and textile industries, being one of the biggest origins of environmental pollution. Photocatalytic degradation is one of the methods that allows the transformation of these pollutants into harmless by-products (Jangid

et al. 2021). A multifunctional fibrous structure that is produced taking into consideration all of these factors, will be an excellent and needed material for the protection of its user against the everyday harmful threats.

Thus, in this work, flax fabrics were functionalized with MgO NPs and MgO–SiO_2 core–shell NPs by in-situ synthesis. The synthesis of the isolated NPs was also tested. A very simple method was used, with water as solvent and low reaction and calcination temperatures (150 °C). The NPs were characterized by Scanning Transmission Electron Microscopy (STEM) and Attenuated Total Reflectance–Fourier–Transform Infrared Spectroscopy (ATR–FTIR) and the functionalized fabrics were characterized by ATR–FTIR, Ground-State Diffuse Reflectance (GSDR), Field Emission Scanning Electron Microscopy (FESEM) and Energy Dispersive X-ray Spectrometry (EDS), which confirmed the successful synthesis of the NPs, as well as the successful incorporation of these NPs onto the flax fabrics. The washing durability of the developed samples was tested. Functional properties like hydrophobicity, UV protection, antibacterial activity (against *Staphylococcus aureus* and *Escherichia coli*) and MB degradation were also evaluated.

Experimental

Materials

The flax fabrics used in this work, with 315 g/m^2 of fabric weight, were supplied by RCS (Braga, Portugal) and produced using 100% flax natural yarns (Bangladesh origin). Magnesium nitrate hexahydrate ($Mg(NO_3)_2{\cdot}6H_2O$) and citric acid were purchase from Scharlau and the ammonia (NH_3) was acquired from AnalaR NORMAPUR. Tetraethyl orthosilicate (TEOS) was obtained from Sigma-Aldrich and the ethanol absolute used was purchased at José Manuel Gomes dos Santos. Memmert UNE 800 oven was used. UV blacklight lamp (15 W) from HQ™ was utilized for photocatalytic tests.

MgO nanoparticles and MgO–SiO_2 core–shell nanoparticles' synthesis

In order to synthetise MgO NPs, $Mg(NO_3)_2$ (0.2 M) was dissolved in distilled water (100 mL) and kept at room temperature under mechanical stirring, until it became clear. Then, citric acid (0.04 M) was added to this solution. Ammonia (NH_3) was added dropwise until a pH of 9 was reached and a precipitate was formed. After 1 h, the obtained MgO NPs were collected by centrifugation at 5000 rpm for 15 min and washed three times with distilled water. Then, they were left to air-dry during two days and were calcinated at 150 °C for 6 h. The addition of the SiO_2 NPs was made keeping the previous process, however, after the 1-h time 50 ml of ethanol and 4 mL of NH_3 were added. Later, 5 mL of a TEOS ethanolic solution (40% vol TEOS in ethanol) were added dropwise, and the mixture was kept under constant stirring, at room temperature for 24 h. At the end, the obtained MgO–SiO_2 core–shell NPs were collected by centrifugation at 5000 rpm for 15 min and washed three times with distilled water. Finally, they were air-dried during two days and were calcinated at 150 °C for 6 h.

Fabrics pre-treatment

Firstly, the flax fabrics (5 cm×5 cm) were washed with 5% (v/v) of a non-ionic detergent at 80 °C for 30 min to remove impurities (waxes, fats, etc.). The fabrics were further cleaned in distilled water at 70 °C for 30 min and dried at 100 °C for 1 h.

Flax fabrics' functionalization with MgO nanoparticles and MgO–SiO_2 core–shell nanoparticles

In-situ synthesis of MgO nanoparticles and MgO–SiO_2 core–shell nanoparticles

For the in-situ synthesis of only the MgO NPs onto the flax fabrics, $Mg(NO_3)_2$ (0.2 M) was dissolved in 100 mL of distilled water and was kept under mechanical stirring at room temperature until it became clear. Then, citric acid (0.04 M) was added to this solution. NH_3 was added dropwise until a pH of 9 was reached and a precipitate was formed. After 1 h, the samples were removed from the solution and heated at 150 °C for 6 h. In order to perform the in-situ synthesis of the MgO–SiO_2 core–shell NPs the process was kept the same as the one referred before, until the end of the 1-h time reaction. Subsequently, 50 ml of ethanol and 4 mL of NH_3 were added. Later, 5 mL of a

TEOS ethanolic solution (40% vol TEOS in ethanol) were added dropwise, and the mixture was kept under constant stirring, at room temperature for 24 h. At the end, the fabric samples were removed from the solution, and heated at 150 °C for 6 h.

Samples characterization

Attenuated total reflectance–fourier transform infrared spectroscopy (ATR–FTIR)

The chemical composition of the synthesized NPs and the functionalized flax fabrics was studied by ATR–FTIR analysis using an IRAffinity-1S, SHIMADZU equipment (Kyoto, Japan). The spectra were obtained in transmittance mode, in the range of 400 to 4000 cm^{-1}. The samples were analysed in 3 different places, to ensure the analysis' homogeneity.

Ground-state diffuse reflectance (GSDR)

The functionalized fabrics were analysed by GSDR. The reflectance and transmittance spectra were recorded using a Spectrophometer UV-2600 (Schimadzu) with the ISR_2600 Plus detector. The equipment was calibrated using as blank barium sulphate (full reflectance).

Five places of the samples were analysed, in order to guarantee the analysis' homogeneity. The reflectance spectra were recorded, in the 200 to 800 nm wavelength, and the remission function was calculated accordingly with the Kubelka–Munk equation:

$$\frac{K}{S} = \frac{[(1-R)]^2}{2 \times R}$$

where K represents the absorption coefficient, S the dispersion coefficient and R the reflectance (Yang and Kruse 2004).

Field emission scanning electron microscopy (FESEM)

The surface of the functionalized fabrics was studied by FESEM using NOVA 200 Nano SEM from FEI Company (Hillsboro, OR, USA). The samples were coated with a thin film (20 nm) of Gold (Au) and Palladium (Pd) before the analysis. The images were taken in topographic mode with an accelerated voltage of 10 kV.

Scanning transmission electron microscopy (STEM)

The morphology of the synthetized NPs was studied by STEM using a NOVA 200 Nano SEM from FEI Company (Hillsboro, OR, USA) with a scanning transmitted electron microscopy detector. The STEM grids were dipped onto an ethanol suspension containing the NPs and then dried.

Wash fastness

The wash durability of the MgO and MgO–SiO_2 nanocoating was evaluated using an adaptation of the standard "ISO6330-Textiles, Domestic Washing and drying, procedures for textile testing", in order to mimic the domestic washing programmes. According to this standard, the agitation speed ranges between 119 and 179 rpm, for delicate and durable press parameters, respectively. Thus, the samples flax, flax + MgO and flax + MgO–SiO_2 were placed in contact with distilled water and centrifugated at 200 rpm for 6 h, continuously. The main goal of this procedure was to infer if the NPs were still fixed onto the fabrics, even after a continuous contact with water under agitation and using a SDC phosphate reference detergent ECE-B with a concentration of 4% (w/v).

To verify if not only the MgO but also the MgO–SiO_2 core–shell nanoparticles were still on the flax surface after the washing tests, the reflectance of the samples was measured in the 200–800 nm range and the remission function was calculated.

Multifunctionality evaluation

Water contact angle measurement

WCA was determined using a Contact Angle System (dataphysics) coupled to a high-resolution camera, in order to evaluate the hydrophobicity of the different functionalized fabric samples. Distilled water (5 µL) was dispensed from the syringe onto the surface of the sample. Ten different places of each sample were measured, and the mean and the standard deviation values were calculated.

UV protection

In order to calculate the UPF and the UVA and UVB blocking values of the developed systems, the transmittance spectra of the samples were recorded in the 280 to 400 nm wavelength range, following EN13758-1, using a Spectrophotometer UV-2600 (Schimadzu) with the ISR_2600 Plus detector. Different places of the samples were analysed, to ensure the homogeneity of the analysis.

Antibacterial activity tests

The antimicrobial activity of MgO NPs and MgO–SiO_2 core–shell NPs solutions was qualitatively determined against *Escherichia coli* CECT 434 (as representative of Gram-negative bacteria) and *Staphylococcus aureus* ATCC 6538 (as representative of Gram-positive bacteria) through the halo inhibition method. Three different NPs' concentrations were assayed: 0.0005 mg/mL, 0.0010 mg/mL and 0.0050 mg/mL. The inoculum was prepared by adding in a sterile medium a portion of the bacterium *S. aureus* or *E. coli* to 40 mL of TSB (Tryptic soy broth). The bacteria grew in an orbital incubator at 37 ºC, with orbital shaking at 120 rpm, overnight (≈ 18 h). Then, the cell suspension was adjusted to a final concentration of approximately 1×10^8 CFU/mL, determined from the optical density at 620 nm.

In the antimicrobial susceptibility test, on a Petri dish containing 15 mL of Plate Count Agar (PCA), 0.1 mL of the bacterial solution (1×10^8 CFU/mL) was spread over the dry agar. After drying, samples of 1×1 cm^2 were placed in the center of each Petri dish on the agar surface and incubated at 37 °C. Measurements of the bacterial growth inhibition zone were taken after 24 h of incubation time. This test was repeated three times in triplicate.

The antimicrobial activity of flax fabrics functionalized with MgO NPs and MgO–SiO_2 core–shell NPs was determined in a quantitative way based on the Absorption method from the internationally recognized Japanese industrial standard (JIS L 1902: 2002, ''Testing method for antibacterial activity of textiles''). The microorganisms assayed were the Gram-positive bacteria *S. aureus* (ATCC 6538) and the Gram-negative bacteria *E. coli* (ATCC 434). Briefly, inocula of *E. coli* and *S. aureus* were prepared in 20.0 ± 0.1 mL of TSB (Tryptic Soy Broth, Merck) and incubated for a period of 18 to 24 h at 37 ± 1 °C under agitation (120 rpm). Subsequently, microbial concentrations were adjusted to 3×10^8 cells/mL via absorbance readings and based on a corresponding calibration curve. An aliquot of each suspension (400 µL) was added to 20 mL of TSB for *E. coli* and *S. aureus* and incubated for 3 h at 37 ± 1 °C. The microbial concentration was again measured and 3×10^5 cells/mL were obtained using a 20-fold dilution of the respective medium (in distilled water). Then, 50 µL of this inoculum was added to each sample. Samples were incubated for 24 h at 37 ± 1 °C, without agitation. Then, 5 mL of physiological saline solution (8.5 g of NaCl and 2.0 g of non-ionic surfactant Tween 20 (Sigma Chemical Co.) per litre) were added to the samples, which were then vortexed (5 times, 5 s each time). The number of living cells was assessed by the serial dilution plate count method. All assays were performed in triplicate and repeated in three independent assays.

The antibacterial activity (%) after 24 h incubation was calculated by the formula:

$$\text{Antibacterial activity}(\%) = [(B - A)/B] \times 100$$

where A represents the number of bacteria in the tested sample after 24 h and B the number of bacteria in the starting suspension before addition of the sample.

Methylene blue degradation

MB was used as a degradation model compound to evaluate the photocatalytic activity of the MgO NPs and MgO–SiO_2 core–shell NPs deposited onto the fabrics. A drop (500 µL) of a MB solution (1 g/L) was placed in the centre of the functionalized fabrics (5×5 cm). The samples were dried and kept in the dark for 10 min, in order to reach the adsorption/desorption equilibrium. Then, they were irradiated by a UV blacklight lamp during 7 h and monitored hourly by GSDR.

Results and discussion

$MgO–SiO_2$ core–shell NPs' synthesis

As mentioned before in an initial phase, MgO and $MgO–SiO_2$ core–shell nanoparticles were synthetized using magnesium nitrate as the precursor, ammonia as the reducing agent and water as solvent. The experimental procedure of this synthesis is summarized in a scheme of Fig. 1.

As can be seen, the procedure was very simple and the conditions used were mild, including the use of water as solvent, low reactions times and only 1 h for the MgO synthesis. Low reactions temperatures were also used, being that the two syntheses were made under room temperature. The calcination temperature used, 150 °C, is much lower than other ones that were used in similar works, being that they are usually between 400 and 550 °C (Hiremath et al. 2017; Das et al. 2018; Pugazhendhi et al. 2019; Fouda et al. 2021).

The addition of the citric acid to the reaction was essential to guarantee the formation of a core–shell structure. The citric acid was added before the synthesis of the SiO_2 shells, in order to increase the zeta potential of the MgO NPs' surface, avoiding the formation of agglomerates. If the core section of the NPs is well dispersed, it's easier to obtain a monodisperse product. Besides this, the positively charged ammonium ions adsorbed onto the MgO surface, with citric acid will attract negatively charged SiO_2 species formed in the reaction more easily, which is very important for the formation of the $MgO–SiO_2$ core–shell structure (Yang et al. 2013).

It's important to notice that the addition of the SiO_2 shell is made by only adding one step to the MgO NPs synthesis, contributing to the simplicity of this procedure. This method is also very versatile, since that by using the same experimental procedure is possible to obtain the isolated NPs but also its in-situ synthesis onto the surface of the flax fabrics.

$MgO–SiO_2$ core–shell NPs' characterization

The ATR–FTIR spectra of the MgO NPs and $MgO–SiO_2$ core–shell NPs are exhibited n Fig. 2a and b.

MgO NPs easily chemisorb water (H_2O) and carbon dioxide (CO_2) molecules when in contact with the atmosphere (Zahir et al. 2019). The sharp peak at approximately 3700 cm^{-1} may be related to $A_{2u}(OH)$ lattice vibration of some residual amount of magnesium hydroxide ($Mg(OH)_2$), that wasn't completely decomposed during calcination or that as formed from the MgO hydrolysis by atmospheric humidity (Li et al. 2014; Ansari et al. 2017; Modwi et al. 2018). The band peaking at around 1465 cm^{-1} can be attributed to the CO_3^{2-} groups adsorbed at the

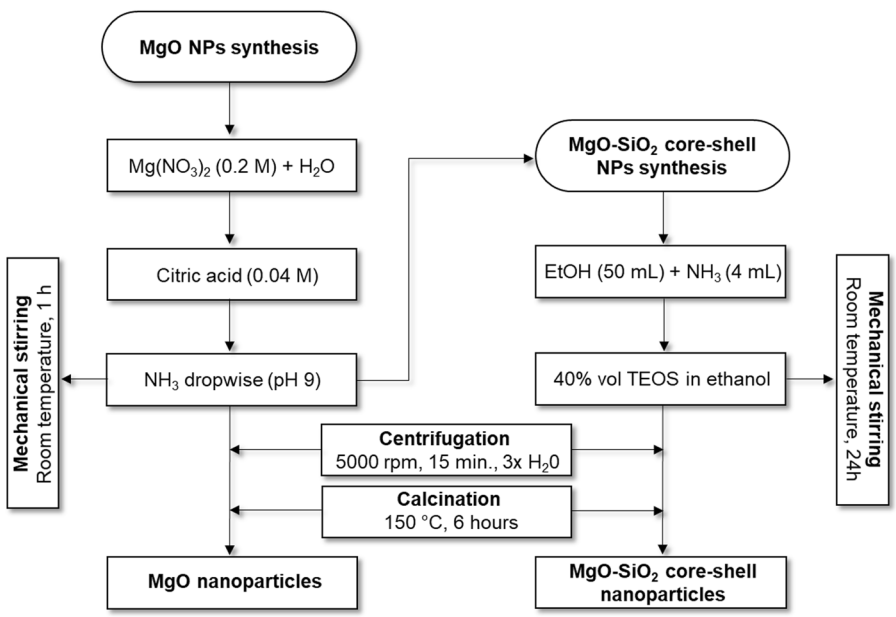

Fig. 1 Schematic diagram of the experimental procedure of the synthesis of MgO NPs and $MgO–SiO_2$ core–shell NPs

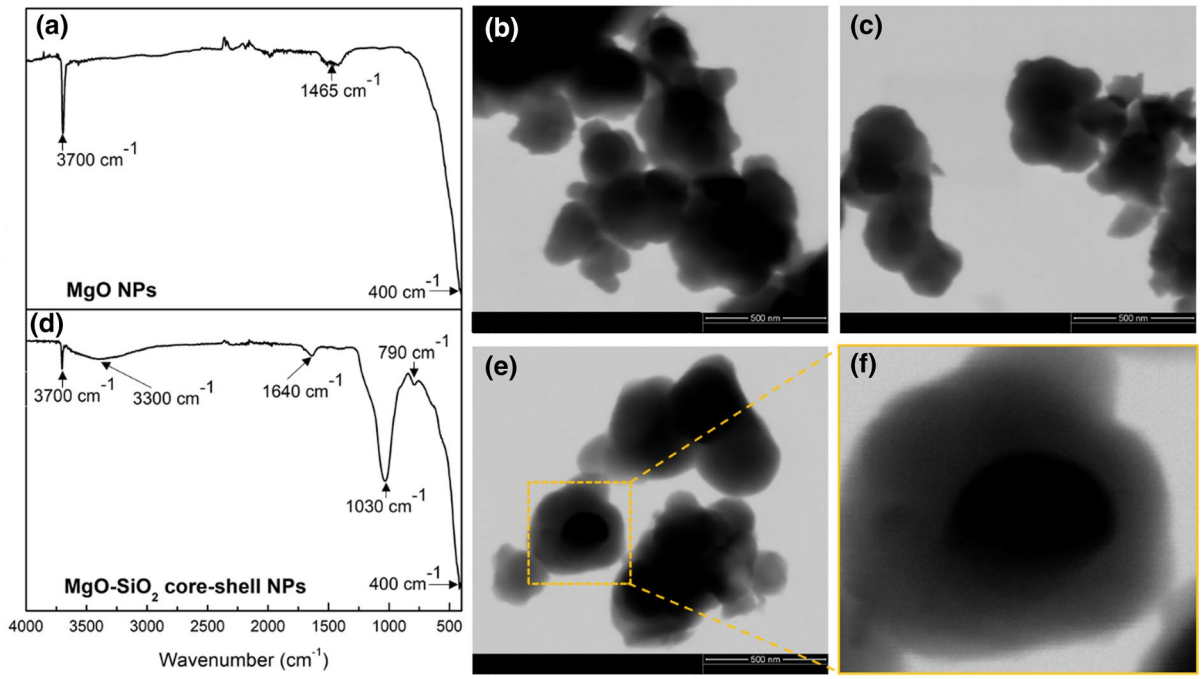

Fig. 2 MgO NPs' and MgO–SiO_2 NPs' characterization: **a** ATR-FTIR spectrum of the synthesized MgO NPs; **b–e** STEM images of the MgO–SiO_2 core–shell NPs (scale bar 500 nm); **f** Zoom image of a portion of image **e**); **d** ATR-FTIR spectrum of the synthesized MgO-SiO_2 core-shell NPs

MgO surface (Mageshwari et al. 2013; Sharma and Kakkar 2017). On the other hand, the band peaking at approximately 400 cm^{-1} is associated to the Mg–O streching vibration, confirming the successful synthesis of MgO NPs (Selvam et al. 2011; Mageshwari et al. 2013; Li et al. 2014) (Fig. 2a)).

In the MgO–SiO_2 core–shell NPs spectrum (Fig. 2d) is posible to observe that the intensity of band peaking at 3700 cm^{-1} is lower than the same band in the MgO NPs spectrum, which means that the coverage and the binding of the MgO NPs with the shell of SiO_2 was made, and the binding of the -OH groups at the Mg^{2+} sites decreased, avoiding the formation of $Mg(OH)_2$ when in contact with atmosphere humidity (Selvam et al. 2011). The small peak at 1640 cm^{-1} is probably related to the O–H bending vibrations of some water molecules adsorbed at the NPs powder (Katumba et al. 2008; Damian et al. 2013).

The wide band at aproximately 3300 cm^{-1}, that was not present in the spectrum a), is probably related to the overlapping of Si–OH and O–H stretching vibrations, confirming the formation of a SiO_2 shell around the MgO NPs, which are hydrogen-bonded (Damian et al. 2013; Hoang et al. 2018). The addition of the shell lead to the appearance of the characteristic bands of SiO_2 NPs, namely the band peaking at 1030 cm^{-1}, related to the Si–O–Si covalent bonds vibrations and the band peaking at 790 cm^{-1}, related to the symmetric stretching vibration of Si–O–Si (Damian et al. 2013; El-Naggar et al. 2017; Araújo et al. 2020). Like the spectrum a), there is a strong band peaking at 400 cm^{-1}, which is characteristic of the Mg–O bond, confirming the presence of a MgO core on the synthesised NPs (Selvam et al. 2011; Mageshwari et al. 2013; Li et al. 2014).

The STEM images of the synthesised MgO–SiO_2 core–shell nanoparticles are exhibited on Fig. 2b–f. It's possible to observe that the developed NPs present a spherical morphology, being that the formation of the core–shell structure is verified since the difference between the internal and external segments of the NPs is very clear. The MgO core of the NPs presents a much darker colour when compared to the SiO_2 shell. The core diameter and the shell thickness were measured by the analysis of the STEM images

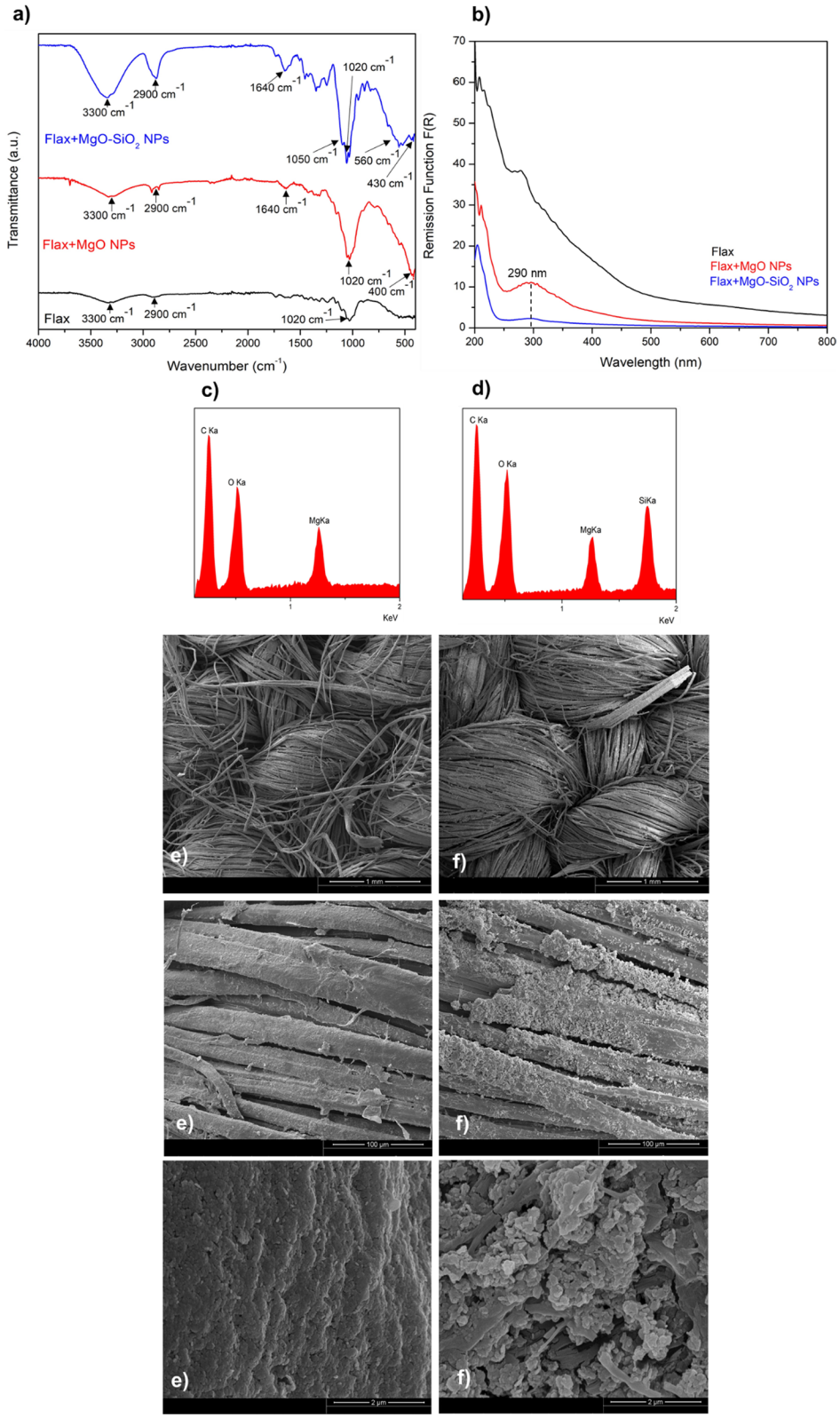
a)
Transmittance (a.u.)
Wavenumber (cm-1)
Flax+MgO-SiO2 NPs
3300 cm-1
2900 cm-1
1640 cm-1
1020 cm-1
1050 cm-1
560 cm-1
430 cm-1
Flax+MgO NPs
3300 cm-1
2900 cm-1
1640 cm-1
1020 cm-1
400 cm-1
Flax
3300 cm-1
2900 cm-1
1020 cm-1
b)
Remission Function F(R)
Wavelength (nm)
290 nm
Flax
Flax+MgO NPs
Flax+MgO-SiO2 NPs
c)
C Ka
O Ka
MgKa
KeV
d)
C Ka
O Ka
MgKa
SiKa
KeV
e)
f)
1 mm
100 µm
2 µm

◂**Fig. 3** Characterization of the flax fabrics functionalized with MgO NPs and MgO–SiO_2 core–shell NPs: **a** ATR-FTIR spectra of the non-functionalized flax fabrics (black) and the flax fabrics functionalized with MgO NPs (red) and MgO–SiO_2 core–shell NPs (blue); **b** GSDR spectra of the non-functionalized flax fabrics (black) and the flax fabrics functionalized with MgO NPs (red) and MgO–SiO_2 core–shell NPs (blue); EDS analysis of the flax fabrics functionalized with **c** MgO NPs and **d** MgO–SiO_2 core–shell NPs; FESEM images of the flax fabrics functionalized with **e)** MgO NPs and **f)** MgO–SiO_2 core–shell NPs (scale bars 1 mm, 100 and 2 µm)

and using the *ImageJ* software. It was verified that the mean diameter of the core was of 128.5 ± 45.0 nm and that thickness of the shell was of 60.8 ± 17.1 nm.

By this analysis of the ATR–FTIR spectra and the STEM images, it was possible to verify that not only the MgO NPs but also the MgO–SiO_2 core–shell NPs were successful synthesised. Consequently, it can be concluded that the addition of the SiO_2 shell to the MgO NPs was effective, being that they were chemically bonded and that a core–shell structure was formed.

Characterization of the flax fabrics functionalized with MgO and MgO–SiO_2 core–shell NPs

The characterization of the flax fabrics functionalized with the MgO NPs and MgO–SiO_2 core–shell NPs is exhibited in Fig. 3.

The ATR–FTIR spectra of the non-functionalized flax as well as the flax functionalized with MgO NPs and MgO–SiO_2 core–shell NPs is presented in Fig. 3a. The flax spectrum shows the characteristic peaks of natural cellulosic fibers, namely cellulose, hemicellulose and lignin. The broad band peaking at approximately 3300 cm^{-1} is related to the O–H stretching vibrations of the hydroxyl groups from cellulose and lignin, but also from some water molecules that may be adsorbed onto the flax fabrics surface (Costa et al. 2018; Araújo et al. 2020). It's also possible to observe a band peaking at around 2900 cm^{-1}, which can be attributed to the asymmetric C–H stretching vibrations of cellulose and hemicellulose and the band peaking at 1200 cm^{-1} is related to the C–O stretching vibrations (Costa et al. 2018; Ferreira et al. 2019; Araújo et al. 2020).

On the other and, on the spectrum of the flax fabrics functionalized with MgO NPs, besides the presence of the bands peaking at 3300, 2900 and 1020 cm^{-1}, related to the flax fibers, is also possible to see the appearance of two new peaks at around 1640 cm^{-1} and 400 cm^{-1}. The band peaking at 1640 cm^{-1} is related to the O–H bending vibration of adsorbed water molecules. It appeared before the fucntionalization, thus the addition of the NPs powder probably increased water absortion (Katumba et al. 2008; Damian et al. 2013). The band located at around 400 cm^{-1} is most likely a result of the Mg–O stretching vibration, confirming the successful functionalization of the flax fabrics with the MgO NPs (Selvam et al. 2011; Mageshwari et al. 2013; Li et al. 2014).

In the Flax + MgO–SiO_2 NPs spectrum, besides the typical bands of flax fabrics and MgO NPs, is also possible to see the appearance of a new band peaking at 1050 cm^{-1}, which is most likely related to the Si–O–Si covalent bonds vibrations, confirming the introduction of the SiO_2 NPs. It's also possible to observe an increase of the intensity of the band peaking at 3300 cm^{-1}, which is most likely related to the stretching vibrations of the O–H and Si–OH bonds, which may indicate that there was the establishment of hydrogen bonds between the hydroxyl groups of the flax and the MgO–SiO_2 core–shell NPs. These results lead to the conclusion that the core–shell NPs are well anchored to the flax fabrics surface, and that the shell of SiO_2 allowed this anchorage. It's also possible to ensure that the functionalization of the flax fabrics with not only the MgO NPs, but also with the MgO–SiO_2 core–shell NPs was successfully accomplished.

Looking at the GSDR spectra of the non-functionalized flax fabrics and the flax fabrics functionalized with MgO NPs and MgO–SiO_2 core–shell NPs (Fig. 3b), is possible to verify that for the fabrics functionalized with MgO NPs, a new band at approximately 290 nm appears. This band can be attributed to the MgO NPs, confirming the successful functionalization of the flax fabrics with these particles (Das et al. 2018; Fouda et al. 2021). It can also be observed that with the addition of the NPs, the absorption band decreased when compared to the band of the non-functionalized flax. This phenomenon can be related to the presence of the NPs' powder onto the fabrics surface, being that the synthesised NPs are inorganic white pigments at nanoscale, and therefore present a high reflective index. Thus, with the NPs' functionalization an increase of the reflectance is expected and

consequently a decrease in the absorption intensity (S Anesh et al. 2015). This also explains why in the spectrum of the flax fabrics functionalized with the MgO–SiO_2 NPs the intensity of the NPs absorption band is lower when compared to the ones functionalized with only MgO NPs, with the addition of the SiO_2 shell, there is an increase of the number of NPs, thus an increase of the reflectance.

Figure 3c and d present the EDS results for the flax fabrics functionalized with MgO NPs and MgO–SiO_2 core–shell NPs, respectively. This analysis allowed us to infer the elemental composition of the samples. It's possible to observe the presence of the magnesium (Mg) and silicon (Si) characteristic peaks for the respective samples, which means that Mg and Si were present onto the flax fabrics.

The surface morphology of the functionalized flax fabrics with the two types of NPs was analysed using FESEM (Fig. 3e and f). Figure 3e shows the distribution of the MgO NPs onto the flax fabrics surface with different magnifications (1 mm, 100 and 2 µm). As it can be seen, the NPs are homogeneously distributed all over the fibers' surface, being that there is the presence of some aggregates and that the particles seem to have a spherical shape. The same can be observed for the fabrics functionalized with MgO–SiO_2 core–shell NPs, but in this case more aggregates can be observed. This is in accordance with what was expected since more particles are present onto the fabrics surface.

Through the ATR–FTIR, GSDR, EDS and FESEM analysis, it can be inferred that the functionalization of flax fabrics with MgO NPs as well as MgO–SiO_2 core–shell NPs was successful, and that the in-situ synthesis of the NPs using the same conditions as the ones used for the isolated NPs is possible. This is very beneficial, because the in-situ synthesis of the NPs is a very simple method that eliminates some steps that are needed in other functionalization techniques and allows the use of lower quantities of solvents and reagents. However, the synthesis of the isolated NPs can be an excellent strategy for the scale-up of this procedure. It's important to notice that this versatile method uses water as solvent and low reaction temperatures and times, as well as a calcination temperature much lower than the other ones reported on literature. The core–shell structure, in this case with a SiO_2 shell, allowed the anchorage of the NPs onto the flax fibers surface, due to the presence of hydrogen bonds between the silanol groups of the SiO_2 and the hydroxyl groups of the flax, which wouldn't happen with only the MgO NPs. Thus, the addition of a core–shell structure to natural fibers can be a great solution for one of the main problems in nano-functionalization of textiles, the effective binding of the NPs onto fabrics' surface.

Wash fastness

The durability of the functionalization of the fabrics with MgO NPs and MgO–SiO_2 core–shell NPs was evaluated. For that purpose, the samples were immersed in distilled water and were centrifugated in order to mimic a domestic washing (like it was described in 2.6). Then, the fabrics were dried, their reflectance was measured by GSDR and the remission function was calculated. The obtained spectra, before and after the washing cycle are represented on Fig. 4a, b and c.

Regarding Flax + MgO sample, it is visible an increase of the MgO characteristic band intensity between 200 and 400 nm after the washing procedure. In fact, with the washing process, some of the NPs that are not well anchored onto the fibers surface will be washed and consequently, the absorbance will increase due to the decrease of the NPs reflectance intensity onto the surface of the fibers. In fact, this washing process is essential to remove the NPs loose on the surface of the fibers, leaving only those that remain strongly anchored to the surface.

However, and by the analysis of the spectra of the flax fabrics functionalized with MgO–SiO_2 core–shell NPs, the spectrum of the samples before and after washing remains practically the same. Thus, the MgO–SiO_2 NPs were more attached to the flax fabrics than the MgO ones, since after the wash the loss of the core–shell NPs was almost unnoticeable. By the FESEM images of Error! Reference source not found. d) and e) it's possible to see that even after the washing procedure, the MgO and MgO–SiO_2 NPs were still present onto the surface of the fabrics, maintaining a similar morphology and distribution as before the wash (Fig. 3e and f). This, in combination with the results obtained for the ATR-FTIR analysis of the functionalized flax fabrics, proves that the SiO_2 shell undoubtedly improved the anchorage of the NPs onto the fabrics' surface. Therefore, the development of a MgO–SiO_2 core–shell structure is very advantageous,

being that a better adhesion of the MgO NPs is obtained, without compromising their excellent properties. The wash fastness was also evaluated using a detergent, as described in 2.6. The obtained spectra of the flax fabrics functionalized with MgO–SiO_2 core–shell NPs before and after the washing cycle with detergent are represented on Fig. 4c. Although with the use of detergent, a big loss of NPs would be expected, it can be observed that the NPs remained strongly attached to the fabrics' surface. As it can be observed, the MgO characteristic band between 200 and 400 nm is still present indicating that even after a washing cycle of 6 h, and using a detergent, the coating of the flax fabrics with the NPs is maintained, which proves its great durability.

Functional properties evaluation

UV protection

An effective UV protection material, that prevents the harmful effects caused by the sun, is of huge importance (Koozekonan et al. 2021). The UV protection behaviour of the developed systems was evaluated, being that the UPF, UVA and UVB blocking values were calculated using the EN13758-1 standard (Table 1).

It's possible to clearly see the improvement of the UPF values with the NPs incorporation, being that this improvement is more accentuated for the fabrics with MgO–SiO_2 core–shell NPs. The UV-blocking capability of metal oxides is well known. This property can be explained by two different theories, one

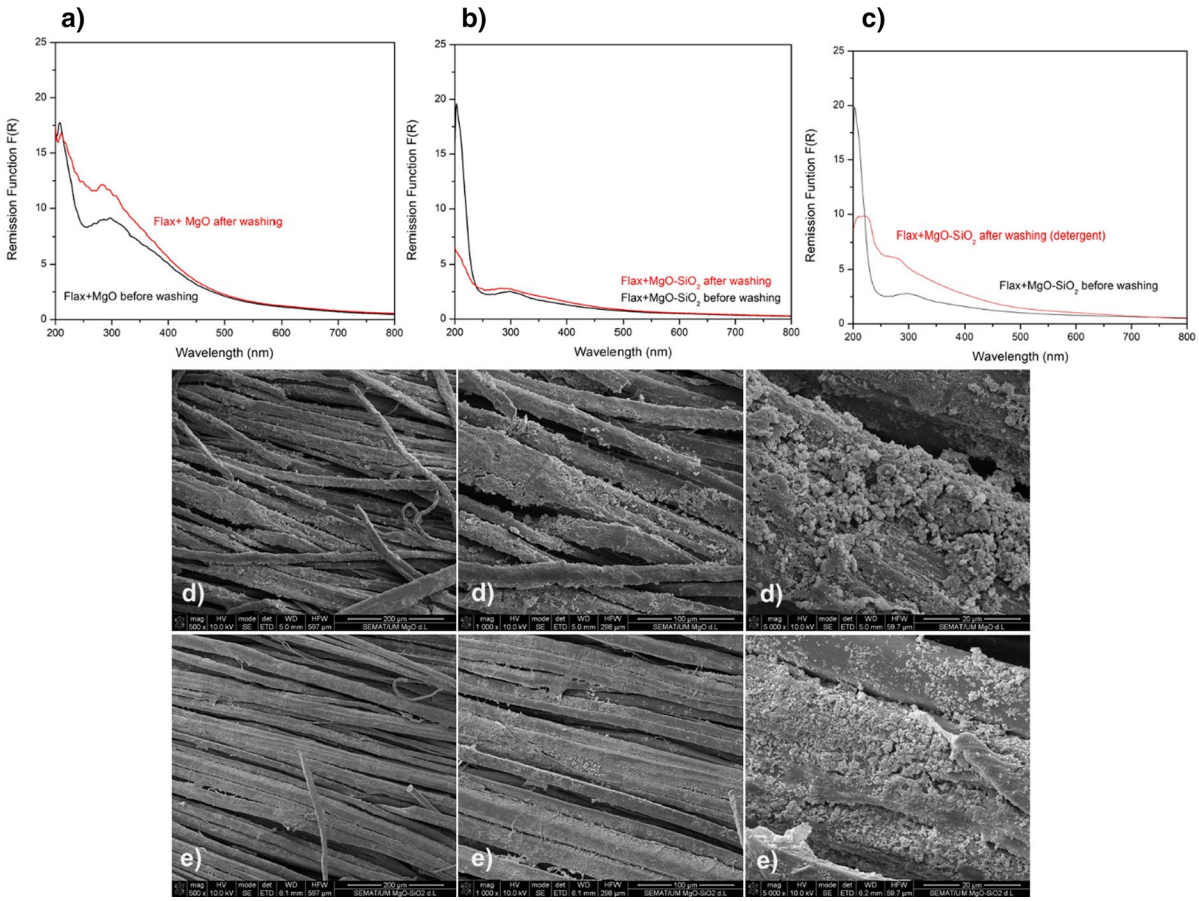

Fig. 4 GSDR spectra of the flax fabrics functionalized with **a** MgO NPs and the **b** MgO–SiO_2 core–shell NPs before and after the wash and **c** flax fabrics functionalized with MgO–SiO_2 core–shell NPs before and after the wash with detergent. **d** FESEM images of the flax fabrics functionalized with **e** MgO and **f** MgO–SiO_2 core–shell NPs after the wash

Table 1 UPF, classification and UVA and UVB blocking (%) values of the flax, flax + MgO and flax + MgO–SiO_2 NPs samples

Sample	UPF	Classification	UVA blocking (%)	UVB blocking (%)
Flax	50	Excellent	97.96	97.95
Flax + MgO	211	Excellent	99.40	99.54
Flax + MgO–SiO_2	530	Excellent	99.73	99.83

states that metal oxide NPs reflects and/or scatters UV rays and the other one explains that the semiconductive properties of this material lead to the absorption of UV radiation (Nair et al. 2018). The UV protection of MgO NPs' coated cotton fabrics was already reported, being that UPF values higher than 50 were obtained (Subramanian et al. 2008). The increase of the UPF value for the fabrics with MgO–SiO_2 core–shell NPs can be explained by the improvement of the MgO properties with the addition of the SiO_2 (Jeelani et al. 2019).

Hydrophobicity properties

In order to study the hydrophobicity of the developed fabrics' surface, the WCA was measured in ten different places of the samples, in order to ensure the homogeneity of the analysis. The results obtained for these measurements are exhibited on Fig. 5.

If a surface presents a WCA value smaller than 90° it's considered hydrophilic, and higher than 90° hydrophobic. In the case of the WCA being bigger than 150°, the surface may be considered superhydrophobic (Boinovich and Emelyanenko 2008).

For the non-functionalized and treated flax fabrics a WCA of 0° was obtained, which means that without the addition of the NPs the surface of the fabrics' is hydrophilic. The functionalization of the fibers with MgO NPs didn't allow the achievement of a hydrophobic surface, being that a WCA of 0° was still obtained. However, with the incorporation of the MgO–SiO_2 core–shell NPs, the WCA increased to a value of 123.0°, meaning that the hydrophobicity limit was largely overcome. So, in this case, we can say that we started with a hydrophilic surface that became hydrophobic with the addition of MgO–SiO_2 core–shell NPs. These results are in accordance with what was expected, being that the hydrophobic character of SiO_2 NPs is well known (Petcu et al. 2017; Araújo et al. 2020).

Antibacterial activity

As core–shell nanoparticles have recently attracted a lot of attention in the field of nanotechnology, in addition to their chemical and physical characterization, it is extremely important to know about their antibacterial properties. Several reports have already demonstrated the antibacterial properties of some bimetallic core shell nanoparticles, such as Au@Ag NPs (Banerjee et al. 2011; Yang et al. 2017b; Ding et al. 2017), and others but, and as far as is our knowledge, MgO NPs and MgO–SiO_2 core–shell

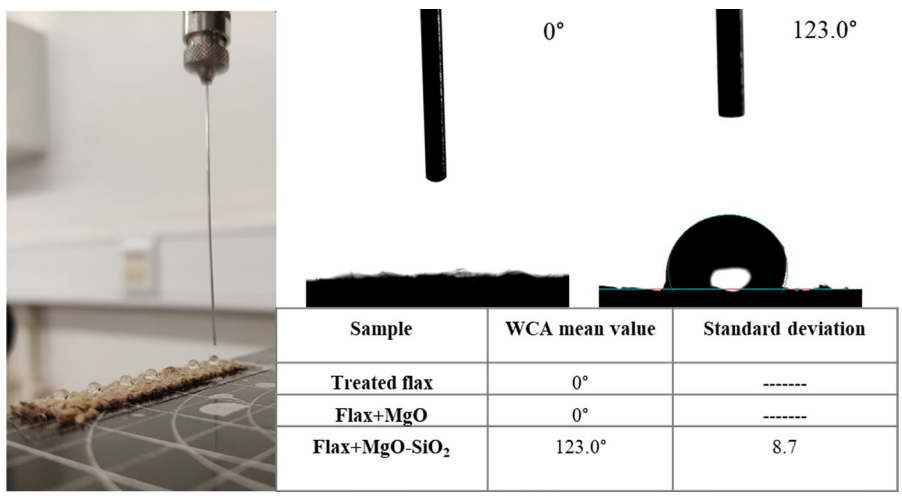

Sample	WCA mean value	Standard deviation
Treated flax	0°	-------
Flax+MgO	0°	-------
Flax+MgO-SiO_2	123.0°	8.7

Fig. 5 WCA values for the treated flax, flax functionalized with MgO NPs and flax functionalized with MgO–SiO_2 core–shell NPs. Image of a flax fabric functionalized with MgO–SiO_2 core–shell NPs

NPs have not yet been studied. Accordingly, in the present study the antibacterial activity of MgO NPs and MgO–SiO_2 core–shell NPs was evaluated against both Gram-positive viz *S. aureus* and Gram-negative viz *E. coli* strains, by the formation of a clear inhibition zone (halo) around the samples, which indicates the absence of bacteria growth. The results are shown in Fig. 6, where the maximum zone of inhibition was obtained for MgO NPs (0,010 mg/mL) for *S. aureus*, while for *E. coli* were obtained at 0.0050 mg/mL concentration (Fig. 6a). The same behavior was observed for MgO–SiO_2 core–shell NPs (Fig. 6b).

Generally, it is accepted that Gram-negative bacteria are more susceptible to NPs than Gram-positive bacteria. It is hypothesized that this may be due to the different cell walls of both. In the case of Gram-negative bacteria, such as *E. coli*, the outer membrane is predominantly constructed from tightly packed lipopolysaccharide (LPS) molecules, followed by a thin (about 2–3 nm) peptidoglycan layer. This arrangement may facilitate the entrance of released ions from NPs into the cell. In contrast, Gram-positive bacteria such as *S. aureus* possess a peptidoglycan layer much thicker than Gram-negative bacteria, spanning over 80 nm with covalently attached teichoic and teichuronic acids. The cell wall destruction that occurs from physical interaction between NPs and the cell wall is more detrimental for Gram-negative bacteria as they lack the thick peptidoglycan layer found in Gram-positive bacteria that could possibly act as a protective layer (Slavin et al. 2017). Moreover, LPS is a unique structure of the cell wall of Gram-negative bacteria that provides a negatively charged region that attracts NPs. This is in accordance with the results of this study where there was a greater antibacterial activity, even slightly, against *E. coli* compared to S. *aureus* obtained with MgO NPs (Fig. 6a) and MgO–SiO_2 (Fig. 6b) core–shell NPs solutions. The same behavior was obtained by Banerjee and co-authors when studied the antibacterial activity Au@Ag core–shell NPs against both Gram negative (*E. coli* and *Pseudomonas aeruginosa*) and Gram positive (*Enterococcus faecalis* and *Pediococcus acidilactici*) bacteria. These authors ascribe this behaviour to the positive charge of the core–shell NPs due to the presence of CTAB as stabilizing agent. Those positively charged core–shell NPs interact more strongly electrostatically with Gram-negative bacteria due to presence of abundant negative charges of lipopolysaccharide thereby killing them more effectively than Gram-positive bacteria (Banerjee et al. 2011).

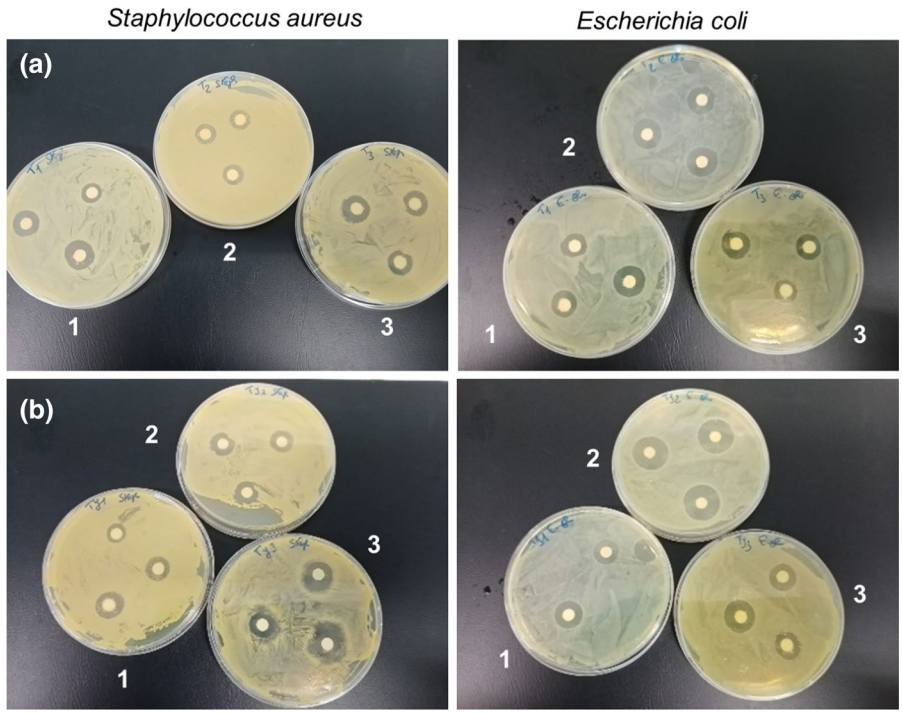

Fig. 6 Comparison of the inhibition zone of **a** MgO NPs and **b** MgO–SiO_2 core–shell NPs solutions against *S. aureus and E. coli* bacteria with different concentrations: (**1**) 0,0005 mg/mL, (**2**) 0,0010 mg/mL and (**3**) 0,0050 mg/mL

Thus, in the present study, in order to try to provide flax fibers antibacterial activity, flax fibers were functionalized with MgO NPs and MgO–SiO_2 core–shell NPs and its antibacterial activity determined. The results are shown in Table 2 where it can be observed that both flax fibers functionalized with NPs showed bactericidal activity against the Gram-positive bacteria *S. aureus* and a bacteriostatic effect against the Gram-negative bacteria *E. coli*.

This means that these materials are capable of completely killing *S. aureus*, but in the case of *E. coli* they just prevent the bacteria from multiplying without destroying it. There was no significant difference between the results obtained for the flax fabrics functionalized with MgO and MgO–SiO_2 core–shell NPs. Nevertheless, these results show that, besides the antibacterial effect of the core–shell NPs solutions, when these NPs are combined onto flax fibers, the antibacterial properties are maintained, allowing for the production of a natural fiber-based textile with antibacterial properties.

Methylene blue degradation

MB was used as the model pollutant (due to its obvious color change) for the evaluation of the photocatalytic activity of the developed samples. In order to do that, 500 µL of a MB solution were dropped onto each sample and kept in the dark for 10 min in order to ensure the adsorption–desorption equilibrium. Then, the samples were exposed to UV radiation for 7 h, being monitored hourly by GSDR (Fig. 7b–d)). The absorbance of the MB solution was also measured (Fig. 7a)).

From the spectrum of the MB solution, it´s possible to infer that this dye presents two characteristic peaks, located at approximately 615 and 664 nm. Comparing the spectrum of the non-functionalized flax with the spectra of the flax functionalized with the two types of NPs, it can be concluded that the characteristic MB peaks intensity decreases faster

Table 2 Antibacterial activity (%) values of flax + MgO and MgO–SiO_2 NPs samples

Sample	*Staphylococcus aureus*	*Escherichia coli*
Flax + MgO	100 ± 0.00	99.88 ± 0.13
Flax + MgO–SiO_2	99.99 ± 0.01	99.42 ± 0.20

Fig. 7 **a** Absorbance spectrum of the MB solution (control); GSDR spectra of the **b** non-functionalized flax, **c** flax functionalized with MgO NPs, **d** flax functionalized with MgO–SiO_2 core–shell NPs in contact with MB after 0, 1, 2, 3, 4, 5, 6, **e** remission function values as a function of time for the 615 nm wavelength and **f** remission function values as a function of time for the 665 nm wavelength

for the functionalized samples. For the 4-h time, the remission function value for the band at 665 nm was of 4.7 for the flax, 2.9 for the flax + MgO and 2.6 for the flax + MgO–SiO_2. Although the MB bands also slightly decrease with time for the flax fabrics, due to its known adsorption capacity (Abutaleb et al. 2020), for the samples with NPs this reduction is faster and more accentuated. This occurrence is most likely related to the photocatalytic activity of the MgO and the MgO–SiO_2 NPs, which results in the degradation of the MB, instead of the adsorption.

The photodegradation of MB by MgO (Bayal and Jeevanandam 2013; Aziz and Karim 2019; Priya et al. 2020) and by NPs coated with SiO_2 (Balu et al. 2018; Fu et al. 2019; El-Sawy et al. 2021) has already been reported. As far as the authors are aware, there is no report on the degradation of MB using MgO–SiO_2 core–shell NPs. However, other works describe the degradation of the dyes by the combination of SiO_2 NPs with other metal oxides. Thus, the mechanism of photocatalytic degradation of the MgO–SiO_2 NPs can be predicted:

$$NPs + hv \rightarrow \left(e^-_{CB} + h^+_{VB}\right) \quad (1)$$

$$e^-_{CB} + O_2 \rightarrow O^{2\cdot -} \quad (2)$$

$$H_2O + O^{2\cdot -} \rightarrow OOH \cdot + OH \quad (3)$$

$$2OOH\cdot \rightarrow O_2 + H_2O_2 \quad (4)$$

$$O^{\cdot -}_2 + dye \rightarrow dye - OO^{\cdot} \quad (5)$$

$$OOH \cdot + H_2O + e^-_{CB} \rightarrow H_2O_2 + OH^- \quad (6)$$

$$H_2O_2 + e^-_{CB} \rightarrow OH^{\cdot} + OH^- \quad (7)$$

$$H_2O_2 + O^{\cdot -}_2 \rightarrow |OH^{\cdot} + OH^- + O_2 \quad (8)$$

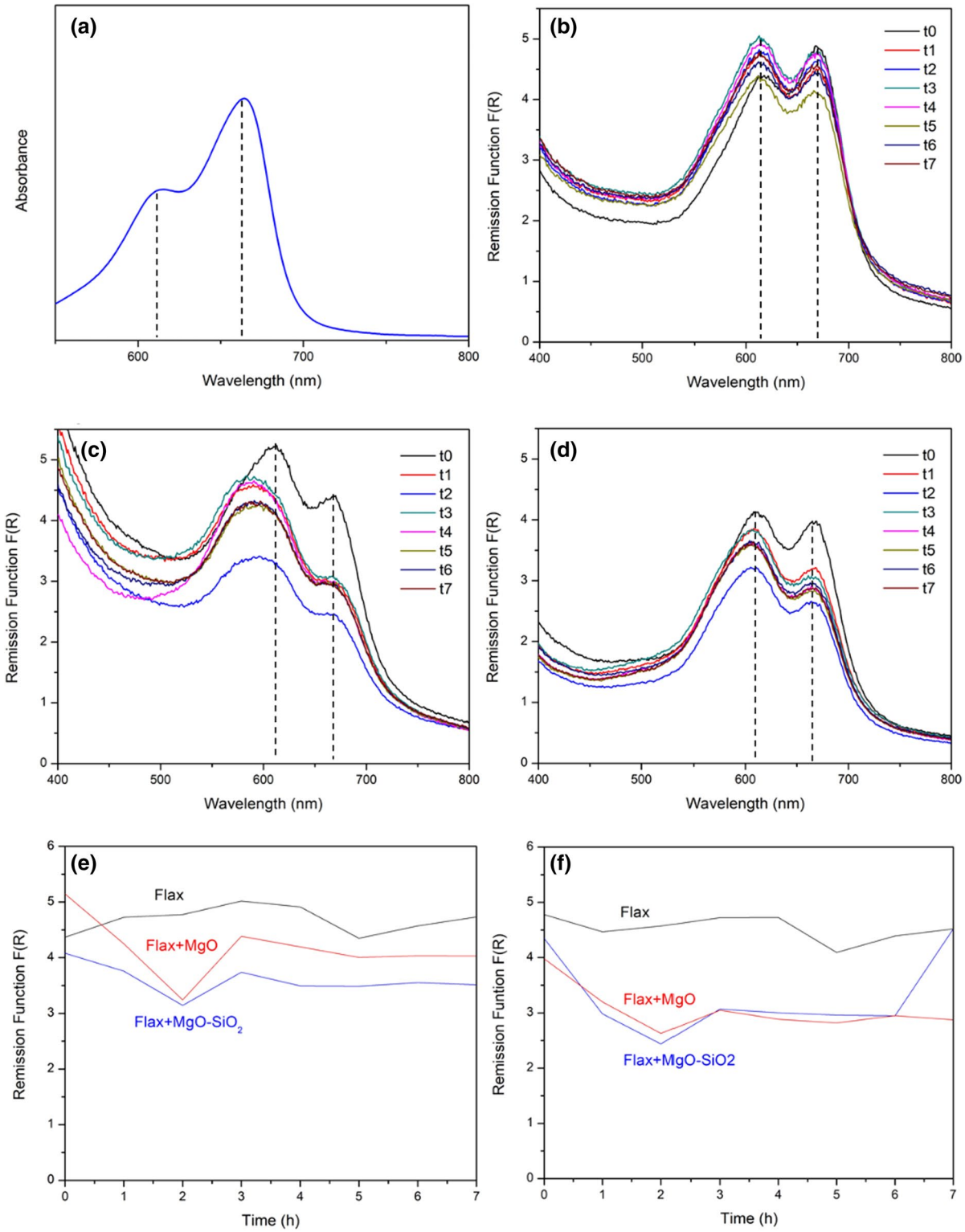
(a)
Absorbance
Wavelength (nm)
(b)
Remission Function F(R)
Wavelength (nm)
t0
t1
t2
t3
t4
t5
t6
t7
(c)
Remission Function F(R)
Wavelength (nm)
(d)
Remission Function F(R)
Wavelength (nm)
(e)
Flax
Flax+MgO
Flax+MgO-SiO2
Remission Function F(R)
Time (h)
(f)
Flax
Flax+MgO
Flax+MgO-SiO2
Remission Funtion F(R)
Time (h)

$$OH^{\cdot}/O_2^{\cdot-}/NPs^{\cdot+} + \text{dye} \rightarrow Dyedegradation \quad (9)$$

Under UV radiation, the NPs molecules are excited, transferring one electron to the conduction band (1). This electron is able to reduce molecular oxygen, originating a super oxide radical (2). Hole-electron pair recombination can be inhibited by the molecular oxygen adsorbed on the surface of the NPs, decreasing the rate of the photocatalytic degradation. The super oxide radical, in the presence of oxygen and organic molecules, can produce hydrogen peroxide or organic peroxide (3,4,5). Another route can generate hydrogen peroxide (6), which can originate hydroxyl radicals, which are powerful oxidizing agents (7,8). These radicals can attack dye molecules, resulting in its degradation (9) (Yang et al. 2017a). These results are already good indicators of the possible potential of these system as photocatalysts for noxious agents. In the future, it will be interesting to evaluate the photocatalytic activity against other toxic chemical compounds.

Conclusions

This work presents the in-situ synthesis of MgO–SiO_2 core–shell NPs onto flax fabrics. This, to the best of the authors knowledge, has not been reported in literature yet. The flax fabrics were functionalized with MgO NPs and MgO–SiO_2 core–shell NPs by a very simple and sustainable in-situ synthesis. The same method, but without the addition of the flax fibers was also performed, in order to obtain the isolated NPs.

ATR-FTIR and STEM were used in order to study the chemical composition and morphology of the synthesized NPs, respectively. The successful synthesis of the MgO NPs and MgO–SiO_2 core–shell NPs was confirmed, as well as the formation of a core–shell structure and the bonding between the MgO core and the SiO_2 shell. ATR-FTIR, GSDR, EDS and FESEM allowed to validate the effective functionalization of the flax fabrics' surface with not only the MgO NPs, but also the MgO–SiO_2 core–shell NPs. It was possible to observe that the NPs were homogenously distributed all over the fabric's surface and that the SiO_2 shell allowed a better anchorage to the flax fibers. The washing durability of the functionalization with MgO NPs and MgO–SiO_2 core–shell NPs was evaluated. It was verified that the MgO–SiO_2 core–shell NPs were more attached to the flax fabrics than the MgO ones, which once again proves that a core–shell structure, with SiO_2 as the shell is very beneficial for the anchorage of the MgO NPs onto the fibers' surface.

The developed samples presented multifunctionality, with UV protection capacity, hydrophobicity, antibacterial activity and MB degradation capability. The functionalized fabrics showed great protection against UV radiation, being that UPF values of 50 + were obtained. The addition of MgO–SiO_2 core–shell NPs onto the fabrics also allowed the achievement of a WCA value of 123.0°, reaching hydrophobicity. The samples also presented a bactericidal effect against *S. aureus* and bacteriostatic effect against *E. coli*. The degradation of harmful chemical agents was also tested, using MB as a model compound. It was verified that the flax fibers functionalized with MgO and MgO–SiO_2 core–shell NPs allowed the possible degradation of the dye in study.

In summary, this works shows the development of a very simple method that allows the synthesis of MgO and MgO–SiO_2 core–shell NPs as well as the in-situ synthesis of these particles onto flax fabrics. The methodologies and the materials used were relatively sustainable, being that when compared to other works in literature, the conditions used were milder. The development of a core–shell nanostructure with SiO_2 turn up to be a great solution for one of the main obstacles of fabrics nano-functionalization, the anchorage of the NPs. The developed samples presented multifunctionality, which makes them excellent candidates for a wide range of applications. In this specific case, these materials show great potential to be used on personal protection applications, being able to actively protect the final user against harmful everyday agents.

Acknowledgments The authors are thankful to project UID/CTM/00264/2022 of 2C2T – Centro de Ciência e Tecnologia Têxtil, funded by National Founds through FCT/MCTES" and to the FCT-Fundação para a Ciência e a Tecnologia PhD Scholarship (grant number SFRH/BD/147812/2019) of Joana Araújo. Diana Ferreira is thankful to CEECIND/02803/2017. Pilar Teixeira is also thankful to FCT, under the scope of the strategic funding of UIDB/04469/2020 unit.

Authors contributions JCA was responsible for the experimental part and wrote the paper. DPF supervised the work and also wrote the paper. PT performed the antibacterial activity tests and participated in the writing of the paper. RF also supervised the work.

Funding The authors are thankful to project UID/CTM/00264/2022 of 2C2T – Centro de Ciência e Tecnologia Têxtil, funded by National Founds through FCT/MCTES" and to the FCT-Fundação para a Ciência e a Tecnologia PhD Scholarship (grant number SFRH/BD/147812/2019) of Joana Araújo. Diana Ferreira is thankful to CEECIND/02803/2017. Pilar Teixeira is also thankful to FCT, under the scope of the strategic funding of UIDB/04469/2020 unit. The authors have not disclosed any funding.

Declarations

Conflict of interest The authors declare no conflicts of interest.

References

Abinaya S, Kavitha HP, Prakash M, Muthukrishnaraj A (2021) Green synthesis of magnesium oxide nanoparticles and its applications: a review. Sustain Chem Pharm 19:100368

Abutaleb A, Tayeb AM, Mahmoud MA et al (2020) Removal and recovery of U(VI) from aqueous effluents by flax fiber: Adsorption, desorption and batch adsorber proposal. J Adv Res 22:153–162. https://doi.org/10.1016/j.jare.2019.10.011

Ansari A, Ali A, Asif M, Uzzaman S (2017) Microwave-assisted MgO NP catalyzed one-pot multicomponent synthesis of polysubstituted steroidal pyridines. New J Chem 42:184–197. https://doi.org/10.1039/C7NJ03742B

Araújo JC, Ferreira DP, Teixeira P, Fangueiro R (2020) In-situ synthesis of CaO and SiO2 nanoparticles onto jute fabrics: exploring the multifunctionality. Cellulose 28:1123–1138. https://doi.org/10.1007/s10570-020-03564-1

Araújo JC, Fangueiro R, Ferreira DP (2021) Protective multifunctional fibrous systems based on natural fibers and metal oxide nanoparticles. Polymers 13:2654

Aziz BK, Karim MAH (2019) Efficient catalytic photodegradation of methylene blue from medical lab wastewater using MgO nanoparticles synthesized by direct precipitation method. React Kinet Mech Catal 128:1127–1139. https://doi.org/10.1007/s11144-019-01677-8

Balu S, Uma K, Pan G-T et al (2018) Degradation of methylene blue dye in the presence of visible light using SiO2@α-Fe2O3 nanocomposites deposited on SnS2 flowers. Mater 11:1030

Banerjee M, Sharma S, Chattopadhyay A, Ghosh SS (2011) Enhanced antibacterial activity of bimetallic gold-silver core-shell nanoparticles at low silver concentration. Nanoscale 3:5120–5125. https://doi.org/10.1039/c1nr10703h

Bayal N, Jeevanandam P (2013) Sol–gel synthesis of SnO2–MgO nanoparticles and their photocatalytic activity towards methylene blue degradation. Mater Res Bull 48:3790–3799. https://doi.org/10.1016/j.materresbull.2013.05.092

Boinovich LB, Emelyanenko AM (2008) Hydrophobic materials and coatings: principles of design, properties and applications. Russ Chem Rev 77:583–600. https://doi.org/10.1070/rc2008v077n07abeh003775

Chaudhuri RG, Paria S (2012) Core/shell nanoparticles : classes, properties, synthesis mechanisms, characterization, and applications. Chem Rev. https://doi.org/10.1021/cr100449n

Chavali MS, Nikolova MP (2019) Metal oxide nanoparticles and their applications in nanotechnology. Springer International Publishing, Berlin

Chirila L, Danila A (2021) Hydrophobic and oleophobic finishes for textiles. In: Innovative and emerging technologies for textile dyeing and finishing. pp 325–372

Costa SM, Ferreira DP, Ferreira A et al (2018) Multifunctional flax fibres based on the combined effect of silver and zinc oxide (Ag / ZnO) nanostructures. Nanomaterials. https://doi.org/10.3390/nano8121069

Damian A, Ciesielczyk F, Nowacka M et al (2013) Fluoroalkylsilane versus alkylsilane as hydrophobic agents for silica and silicates. J Nanomater. https://doi.org/10.1155/2013/631938

Das B, Moumita S, Ghosh S et al (2018) Biosynthesis of magnesium oxide (MgO) nanoflakes by using leaf extract of Bauhinia purpurea and evaluation of its antibacterial property against Staphylococcus aureus. Mater Sci Eng C 91:436–444. https://doi.org/10.1016/j.msec.2018.05.059

Ding X, Yuan P, Gao N et al (2017) Au-Ag core-shell nanoparticles for simultaneous bacterial imaging and synergistic antibacterial activity. Nanomedicine 13:297–305. https://doi.org/10.1016/j.nano.2016.09.003

El-Naggar ME, Hassabo AG, Mohamed AL, Shaheen TI (2017) Surface modification of SiO2 coated ZnO nanoparticles for multifunctional cotton fabrics. J Colloid Interface Sci 498:413–422

El-Sawy AM, Gemeay AH, Helal AS, Salem MA (2021) Catalytic degradation of methylene blue in aqueous solution by H2O2 and SiO2-NH2-Cu(II)@SiO2 nanoparticles as catalyst. J Mol Liq 341:117422. https://doi.org/10.1016/j.molliq.2021.117422

Ferreira DP, Ferreira A, Fangueiro R (2018) Searching for natural conductive fibrous structures via a green sustainable approach based on jute fibers and silver nanoparticles. Polymers. https://doi.org/10.3390/polym10010063

Ferreira DP, Costa SM, Felgueiras HP, Fangueiro R (2019) Smart and sustainable materials for military applications based on natural fibres and silver nanoparticles. Key Eng Mater 812:66–74. https://doi.org/10.4028/www.scientific.net/KEM.812.66

Fouda A, Hassan SE-D, Saied E, Hamza MF (2021) Photocatalytic degradation of real textile and tannery effluent using biosynthesized magnesium oxide nanoparticles (MgO-NPs), heavy metal adsorption, phytotoxicity, and antimicrobial activity. J Environ Chem Eng 9:105346. https://doi.org/10.1016/j.jece.2021.105346

Fu N, Ren X, Wan J (2019) Preparation of Ag-coated SiO_2@TiO_2 core-shell nanocomposites and their photocatalytic applications towards phenol and methylene blue degradation. J Nanomater 2019:8175803. https://doi.org/10.1155/2019/8175803

Gunathilake C, Jaroniec M (2014) Mesoporous calcium oxide-silica and magnesium oxide-silica composites for CO2 capture at ambient and elevated temperatures. J Mater Chem A 2:843–852. https://doi.org/10.1158/0008-5472.CAN-05-1818

Hiremath V, Shavi R, Gil Seo J (2017) Mesoporous magnesium oxide nanoparticles derived via complexation-combustion

for enhanced performance in carbon dioxide capture. J Colloid Interface Sci 498:55–63. https://doi.org/10.1016/j.jcis.2017.03.046

Hoang HT, Sertsova AA, Marakulin SI et al (2018) Manufacture of magnesium oxide nanoparticles coated with silica shells. Russ J Inorg Chem 63:1414–1418. https://doi.org/10.1134/S0036023618110074

Jangid NK, Jadoun S, Yadav A et al (2021) Polyaniline-TiO2-based photocatalysts for dyes degradation. Polym Bull 78:4743–4777. https://doi.org/10.1007/s00289-020-03318-w

Jeelani PG, Mulay P, Venkat R, Ramalingam C (2019) Multifaceted application of silica nanoparticles. A review. Silicon

Karthikeyan C, Sisubalan N, Sridevi M et al (2021) Biocidal chitosan-magnesium oxide nanoparticles via a green precipitation process. J Hazard Mater 411:124884. https://doi.org/10.1016/j.jhazmat.2020.124884

Katumba G, Mwakikunga BW, Mothibinyane TR (2008) FTIR and Raman spectroscopy of carbon nanoparticles in SiO 2, ZnO and NiO matrices. Nanoscale Res Lett 3:421–426

Koozekonan AG, Esmaeilpour MRM, Kalantary S et al (2021) Fabrication and characterization of PAN/CNT, PAN/TiO2, and PAN/CNT/TiO2 nanofibers for UV protection properties. J Text Inst 112:946–954. https://doi.org/10.1080/00405000.2020.1813408

Li L-X, Xu D, Li X-Q et al (2014) Excellent fluoride removal properties of porous hollow MgO microspheres. New J Chem 38:5445–5452

Mageshwari K, Mali SS, Sathyamoorthy R, Patil PS (2013) Template-free synthesis of MgO nanoparticles for effective photocatalytic applications. Powder Technol 249:456–462

Modwi A, Khezami L, Taha KK, Idriss H (2018) Flower buds like MgO nanoparticles: from characterisation to indigo carmine elimination. Zeitschrift Für Naturforsch A 73:975–983

Nair S, Nagarajappa GB, Pandey KK (2018) UV stabilization of wood by nano metal oxides dispersed in propylene glycol. J Photochem Photobiol B Biol 183:1–10. https://doi.org/10.1016/j.jphotobiol.2018.04.007

Petcu C, Purcar V, Spătaru C-I, et al (2017) The influence of new hydrophobic silica nanoparticles on the surface properties of the films obtained from bilayer hybrids. Nanomater 7

Prabha S, Durgalakshmi D, Rajendran S, Lichtfouse E (2021) Plant-derived silica nanoparticles and composites for biosensors, bioimaging, drug delivery and supercapacitors: a review. Environ Chem Lett 19:1667–1691. https://doi.org/10.1007/s10311-020-01123-5

Priya R, Stanly S, Kavitharani T, Faruq M, Suresh S (2020) Highly effective photocatalytic degradation of methylene blue using PrO2–MgO nanocomposites under UV light. Optik (stuttg) 206:164318. https://doi.org/10.1016/j.ijleo.2020.164318

Pugazhendhi A, Prabhu R, Muruganantham K et al (2019) Anticancer, antimicrobial and photocatalytic activities of green synthesized magnesium oxide nanoparticles (MgONPs) using aqueous extract of Sargassum wightii. J Photochem Photobiol B Biol 190:86–97. https://doi.org/10.1016/j.jphotobiol.2018.11.014

Rivero PJ, Urrutia A, Goicoechea J, Arregui FJ (2015) Nanomaterials for functional textiles and fibers. Nanoscale Res Lett 10:501. https://doi.org/10.1186/s11671-015-1195-6

Selvam NCS, Kumar RT, Kennedy LJ, Vijaya JJ (2011) Comparative study of microwave and conventional methods for the preparation and optical properties of novel MgO-micro and nano-structures. J Alloys Compd 509:9809–9815. https://doi.org/10.1016/j.jallcom.2011.08.032

Sharma L, Kakkar R (2017) Hierarchical porous magnesium oxide (Hr-MgO) microspheres for adsorption of an organophosphate pesticide: kinetics, isotherm, thermodynamics, and DFT studies. ACS Appl Mater Interfaces 9:38629–38642

Slavin YN, Asnis J, Häfeli UO, Bach H (2017) Metal nanoparticles: understanding the mechanisms behind antibacterial activity. J Nanobiotechnology 15:65. https://doi.org/10.1186/s12951-017-0308-z

Soumya S, Mohamed AP, Mohan K, Ananthakumar S (2015) Enhanced near-infrared reflectance and functional characteristics of Al-doped ZnO nano-pigments embedded PMMA coatings. Sol Energy Mater Sol Cells 143:335–346. https://doi.org/10.1016/j.solmat.2015.07.012

Subramanian K, Dsouza L, Dhurai B (2008) A comparative study of multifunctional finishing of cotton and P/C blended fabrics treated with titanium dioxide/zinc oxide nanoparticles. Indian J Sci Technol 1:1–12

Vu A, Ho K, Lee C (2016) Removal of gaseous sulfur and phosphorus compounds by carbon-coated porous magnesium oxide composites. Chem Eng J 283:1234–1243. https://doi.org/10.1016/j.cej.2015.08.083

Wahab R, Ahmad N, Alam M, Ansari AA (2018) Nanocubic magnesium oxide: towards hydrazine sensing. Vacuum 155:682–688. https://doi.org/10.1016/j.vacuum.2018.06.026

Yang L, Kruse B (2004) Revised Kubelka – Munk theory. I. Theory and application. J Opt Soc Am 21:1933–1941

Yang X, Zhao N, Zhou Q et al (2013) Precise preparation of highly monodisperse ZrO2@SiO2 core–shell nanoparticles with adjustable refractive indices. J Mater Chem C 1:3359–3366. https://doi.org/10.1039/C3TC30324A

Yang C, Dong W, Cui G et al (2017a) Highly efficient photocatalytic degradation of methylene blue by P2ABSA-modified TiO 2 nanocomposite due to the photosensitization synergetic effect of TiO 2 and P2ABSA. RSC Adv 7:23699–23708. https://doi.org/10.1039/C7RA02423A

Yang L, Yan W, Wang H et al (2017b) Shell thickness-dependent antibacterial activity and biocompatibility of gold@silver core–shell nanoparticles. RSC Adv 7:11355–11361. https://doi.org/10.1039/C7RA00485K

Yu W, Li X, He J et al (2021) Graphene oxide-silver nanocomposites embedded nanofiber core-spun yarns for durable antibacterial textiles. J Colloid Interface Sci 584:164–173. https://doi.org/10.1016/j.jcis.2020.09.092

Zahir M, Rahman MM, Irshad K, Rahman MM (2019) Shape-stabilized phase change materials for solar energy storage: MgO and Mg (OH) 2 mixed with polyethylene glycol. Nanomaterials 9:1773